Canadian Geotechnical Journal, Vol. 47, No. 7, pp. 791-805, 2010

On the "elastic" stiffness in a high-cycle accumulation model for sand: a comparison of drained and undrained cyclic triaxial tests

T. Wichtmann[i)], A. Niemunis[ii)], Th. Triantafyllidis[iii)]

Abstract

High-cycle accumulation (HCA) models may be used for the prediction of settlements or stress relaxation in soils due to a large number ($N > 10^3$) of cycles with a relative small amplitude ($\varepsilon^{\mathrm{ampl}} < 10^{-3}$). This paper presents a discussion of the stiffness E used in the basic constitutive equation $\dot{\boldsymbol{\sigma}}' = \mathsf{E} : (\dot{\boldsymbol{\varepsilon}} - \dot{\boldsymbol{\varepsilon}}^{\mathrm{acc}} - \dot{\boldsymbol{\varepsilon}}^{\mathrm{pl}})$ of a HCA model. E interrelates the "trends" of stress and strain evolution. For the experimental assessment of the bulk modulus $K = \dot{u}/\dot{\varepsilon}_v^{\mathrm{acc}}$ the rate $\dot{u}$ of pore water pressure accumulation in undrained cyclic triaxial tests and the rate of volumetric strain accumulation $\dot{\varepsilon}_v^{\mathrm{acc}}$ in drained cyclic tests have been compared. The pressure-dependent bulk modulus K was quantified from fifteen pairs of drained and undrained tests with different consolidation pressures and stress amplitudes. It is demonstrated that both the curves $\varepsilon_v^{\mathrm{acc}}(N)$ in the drained tests and $u(N)$ in the undrained tests are well predicted by the author's HCA model if the elastic stiffness is determined in a way described in the present paper. A simplified determination of K from the un- and reloading curve in an oedometric compression test is discussed.

Key words: High-cycle accumulation model, stiffness E, bulk modulus K, stress relaxation, drained cyclic triaxial tests, undrained cyclic triaxial tests

1 Introduction

A so-called high- or poly-cyclic loading, that means a loading with a large number of cycles ($N > 10^3$) and relative small strain amplitudes ($\varepsilon^{\mathrm{ampl}} < 10^{-3}$) is of practical relevance for many problems in geotechnical engineering. Machine foundations are subjected to many small cycles with constant amplitude. The cyclic loading of the foundations of tanks, silos and watergates is caused by the changing height of the filling. Wind and wave loading causes a high-cyclic loading of the foundations of onshore- and offshore wind power plants. This loading may be multiaxial since the directions and frequencies of the wind and wave loading may be different. This topic is of high actuality for example in connection with a large number of offshore wind parks planned in the North Sea. Another example for a high-cyclic loading are foundations subjected to traffic loading (e.g. railways of high-speed trains or magnetic levitation trains). In that case the strain loops in the soil are also multiaxial due to the moving loads.

A high-cyclic loading may not only cause an accumulation of permanent deformations (e.g. settlements) in the soil but it may also lead to residual changes of the average stress. For example, the shaft resistance of a pile in sand usually decreases with N because the normal stress acting on the shaft relaxates. If the sand is water-saturated and the cyclic loading is applied under nearly undrained conditions, then the pore water pressure accumulates and the mean effective stress $p = \mathrm{tr}\,(\boldsymbol{\sigma}')/3$ decreases. In the extreme case the sand "liquefies" ($\boldsymbol{\sigma}' = \mathbf{0}$).

The finite element (FE) method in combination with a special "explicit" (N-type) calculation strategy (Section 2) and a high-cycle accumulation (HCA) model (Section 3) may be used to predict permanent deformations or stress relaxation due to a high-cyclic loading. The method may be used to solve the problems addressed above involving a high-cyclic loading. The basic assumption of the HCA model proposed by Niemunis et al. [4] is that the strain path and the stress path that result from a high-cyclic loading can be decomposed into an oscillating part and a trend. The oscillating part is described by the strain amplitude. The model predicts primarily the trend (accumulation) of strain $\dot{\boldsymbol{\varepsilon}}^{\mathrm{acc}}$. Depending on the boundary conditions, the cumulative trend can be observed both in the effective stress (pseudo-relaxation) and in strain (pseudo-creep). These trends are interrelated by

$$\dot{\boldsymbol{\sigma}}' = \mathsf{E} : (\dot{\boldsymbol{\varepsilon}} - \dot{\boldsymbol{\varepsilon}}^{\mathrm{acc}} - \dot{\boldsymbol{\varepsilon}}^{\mathrm{pl}}) \tag{1}$$

with the rate $\dot{\boldsymbol{\sigma}}'$ of the effective stress $\boldsymbol{\sigma}'$ (compression positive), the strain rate $\dot{\boldsymbol{\varepsilon}}$ (compression positive), the given accumulation rate $\dot{\boldsymbol{\varepsilon}}^{\mathrm{acc}}$, a plastic strain rate $\dot{\boldsymbol{\varepsilon}}^{\mathrm{pl}}$ (for stress paths touching the yield surface) and an elastic stiffness E. In the context of HCA models "rate" means the derivative with respect to the number of cycles N (instead of time t), i.e. $\dot{\sqcup} = \partial \sqcup / \partial N$. In this paper the total stress is denoted by $\boldsymbol{\sigma} = \boldsymbol{\sigma}' + u\mathbf{1}$ with pore water pressure u. Note that the index $\sqcup^{\mathrm{av}}$ for average (= trend) is omitted in this paper.

A large number of drained cyclic element tests [10–14] has been performed on a medium coarse sand in order to

[i)] Research Assistant, Institute of Soil Mechanics and Rock Mechanics, University of Karlsruhe, Germany (corresponding author). Email: torsten.wichtmann@ibf.uka.de

[ii)] Research Assistant, Institute of Soil Mechanics and Rock Mechanics, University of Karlsruhe, Germany

[iii)] Professor and Director of the Institute of Soil Mechanics and Rock Mechanics, University of Karlsruhe, Germany

develop suitable equations for $\dot{\boldsymbol{\varepsilon}}^{\mathrm{acc}}$ in Eq. (1). These equations are introduced in Section 3. The results from the axisymmetric tests have been generalized to the full tensorial formulation of the HCA model. For the boundary value problems (BVPs) studied so far, the deformations were of essential importance (e.g. FE calculations of settlements of shallow foundations on dry sand [10]). Less attention was paid to an appropriate formulation of E, because the evolution of the trend of stress $\dot{\boldsymbol{\sigma}}'$ was less important in the applications considered first. However, for some BVPs considerable changes of the average stress are expected (e.g. piles under cyclic loading). A closer inspection of E becomes necessary. It is the objective of the present paper.

At present a simple isotropic stiffness $\mathsf{E} = \lambda \mathbf{1} \otimes \mathbf{1} + 2\mu \mathsf{I}$ is used with the Lamé-constants $\lambda = E\nu/(1+\nu)/(1-2\nu)$ and $\mu = G = E/2/(1+\nu)$. The identity tensor I is defined as $I_{ijkl} = \frac{1}{2}(\delta_{ik}\delta_{jl} + \delta_{il}\delta_{jk})$ with Kronecker's symbol δ_{ij}. Therein E is Young's modulus, G is the shear modulus and ν is Poisson's ratio. For Young's modulus E, a pressure-dependent expression

$$E = A\,(p^{\mathrm{atm}})^{1-n}\,(p^{\mathrm{av}})^{n} \tag{2}$$

with the atmospheric pressure $p^{\mathrm{atm}} = 100$ kPa and two dimensionless positive constants A and n is used. Note that E need not be hyperelastic contrary to the implicit models for cyclic loading because it interrelates accumulation trends and not stress and strain rates. The magnitude of E has been roughly estimated.

No systematic experimental study of E in Eq. (1) can be found in the literature either. Some information about the magnitude of E can be found in the paper of Sawicki [6]. He studied pore pressure accumulation and liquefaction phenomena at the Izmit Bay coastal area (Turkey) during the strong earthquake in August 1999. Sawicki used bulk moduli K between 145 and 156 MPa in his compaction model (for its critical review see [10]). These values were obtained from the un- and reloading curves in oedometric tests. Sawicki assumed that these values can be used for the "elastic" stiffness in HCA models. Although being plausible, no experimental evidence has been provided for this assumption yet.

Assuming an isotropic E, the following questions may be posed:

- Which values of ν and E are adequate?
- Is E strongly pressure-dependent?
- Does E depend on amplitude and void ratio?
- For a simplified procedure, can E be determined from the un- and re-loading curve of an oedometric test or is it similar to a small-strain stiffness (i.e. attainable from a resonant column test or from wave velocity measurements)?

The present paper concentrates on K which influences the rate of stress relaxation. Based on the results of 15 pairs of drained and undrained cyclic tests performed on a medium coarse sand the magnitude and the pressure-dependence of K will be discussed. It will be shown that K is slightly amplitude-dependent within the range of amplitudes studied herein.

2 "Explicit" calculation strategy

For predictions of permanent deformations or stress relaxation due to cyclic loading by means of the finite element (FE) method, a conventional *pure implicit* calculation with a $\dot{\boldsymbol{\sigma}}'$-$\dot{\boldsymbol{\varepsilon}}$ constitutive model (e.g. elastoplastic multi-surface models, endochronic models or hypoplastic models) is suitable only for small numbers of cycles ($N < 50$). For large N-values the numerical error becomes excessive in such calculations (Niemunis et al. [4]).

For a high-cyclic loading another strategy of calculation is necessary. It is illustrated in Fig. 1 for the case of a shallow foundation under cyclic loading. Only a few cycles are calculated *implicitly* with small increments $\dot{\boldsymbol{\sigma}}'(\dot{\boldsymbol{\varepsilon}})\Delta t$ using a $\dot{\boldsymbol{\sigma}}'$-$\dot{\boldsymbol{\varepsilon}}$ constitutive model. Larger packages of cycles in between are treated *explicitly*. The *explicit* mode requires a special constitutive formulation (HCA model) which takes packages of cycles ΔN as input. The accumulation of residual strain $\dot{\boldsymbol{\varepsilon}}^{\mathrm{acc}}\Delta N$ due to a package of ΔN cycles of a given strain amplitude $\varepsilon^{\mathrm{ampl}}$ is treated similarly as a creep deformation due to time increments Δt in viscoplastic models. The number of cycles N just replaces the time t. Without tracing the oscillating strain path during the individual cycles, the explicit mode calculates directly the accumulation rate $\dot{\boldsymbol{\varepsilon}}^{\mathrm{acc}}$ which enters the constitutive equation (1).

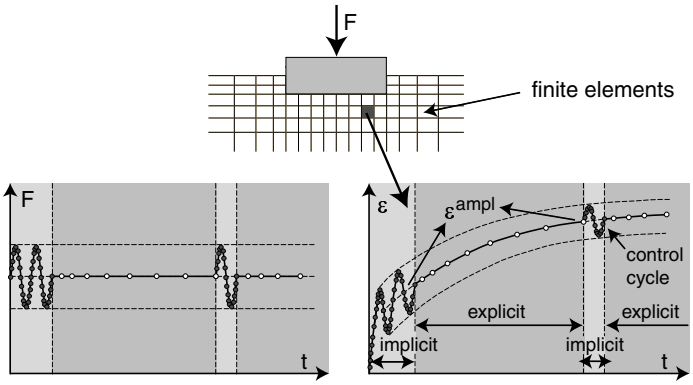

Fig. 1: *FE calculation of the settlements of a shallow foundation under cyclic loading using a combined implicit and explicit calculation*

The implicit parts of the calculation are necessary in order to determine or correct the spatial field of the strain amplitude $\varepsilon^{\mathrm{ampl}}$. The strain amplitude is an important input parameter of the HCA model (Section 3). The first cycle may be *irregular* since the deformations in the first cycle can significantly differ from those in the subsequent cycles (e.g. for a freshly pluviated sand). Therefore the second cycle is used for the determination of $\varepsilon^{\mathrm{ampl}}$. The strain amplitude is determined from the strain path $\boldsymbol{\varepsilon}(t)$ recorded in each integration point during the second cycle. The procedure described by Niemunis [2] is applied. During the explicit parts of the calculation the strain amplitude $\varepsilon^{\mathrm{ampl}}$ is assumed constant. After several thousand cycles the spatial field of the real strain amplitude may have changed due to a compaction and a re-distribution of stress. The explicit calculation should be therefore interrupted and $\varepsilon^{\mathrm{ampl}}$ should be recalculated implicitly (*control cycles*, Fig. 1).

3 HCA model

For $\dot{\boldsymbol{\varepsilon}}^{\mathrm{acc}}$ in Eq. (1) the HCA model proposed by the authors (Niemunis et al. [4]) uses

$$\dot{\boldsymbol{\varepsilon}}^{\mathrm{acc}} = \dot{\varepsilon}^{\mathrm{acc}}\,\mathbf{m} \tag{3}$$

with the "direction" of strain accumulation $\mathbf{m} = \dot{\boldsymbol{\varepsilon}}^{\mathrm{acc}}/\|\dot{\boldsymbol{\varepsilon}}^{\mathrm{acc}}\|$ (flow rule, unit tensor) and the intensity $\dot{\varepsilon}^{\mathrm{acc}} = \|\dot{\boldsymbol{\varepsilon}}^{\mathrm{acc}}\|$. The flow rule of the modified Cam clay (MCC) model

$$\mathbf{m} = \left[\frac{1}{3}\left(p - \frac{q^2}{M^2 p}\right)\mathbf{1} + \frac{3}{M^2}\boldsymbol{\sigma}'^{*}\right]^{\rightarrow} \tag{4}$$

approximates well the ratios $\dot{\varepsilon}_v^{\mathrm{acc}}/\dot{\varepsilon}_q^{\mathrm{acc}}$ measured in drained cyclic triaxial tests and has been adopted in the HCA model. For the triaxial case the Roscoe's stress invariants are $p = (\sigma_1' + 2\sigma_3')/3$ and $q = \sigma_1' - \sigma_3'$ with σ_1' and σ_3' being the axial and lateral effective stress components, respectively. The strain invariants are $\varepsilon_v = \varepsilon_1 + 2\varepsilon_3$ (volumetric strain) and $\varepsilon_q = 2/3(\varepsilon_1 - \varepsilon_3)$ (deviatoric strain). For triaxial extension $\eta = q/p < 0$ a small modification $M = F\ M_c$ is used in Eq. (4) to make it consistent with the Coulomb criterion:

$$F = \begin{cases} 1 + M_e/3 & \text{for } \eta \le M_e \\ 1 + \eta/3 & \text{for } M_e < \eta < 0 \\ 1 & \text{for } \eta \ge 0 \end{cases} \tag{5}$$

wherein

$$M_c = \frac{6\sin\varphi_c}{3 - \sin\varphi_c} \quad \text{and} \quad M_e = -\frac{6\sin\varphi_c}{3 + \sin\varphi_c}. \tag{6}$$

In Eq. (4), $\sqcup^{\rightarrow}$ denotes Euclidean normalization and $\boldsymbol{\sigma}'^{*}$ is the deviatoric part of the effective stress.

The intensity of strain accumulation $\dot{\varepsilon}^{\mathrm{acc}}$ in Eq. (3) is calculated as a product of six functions:

$$\dot{\varepsilon}^{\mathrm{acc}} = f_{\mathrm{ampl}}\ \dot{f}_N\ f_e\ f_p\ f_Y\ f_\pi \tag{7}$$

Each function (Table 1) takes into account a different influencing parameter. The function f_{ampl} describes the dependence of $\dot{\varepsilon}^{\mathrm{acc}}$ on the strain amplitude $\varepsilon^{\mathrm{ampl}}$. Actually the model incorporates a tensorial definition of the amplitude for multidimensional strain loops [4]. It is applicable to convex (e.g. elliptical) six-dimensional strain loops. Here we use the scalar measure $\varepsilon^{\mathrm{ampl}}$ of this tensorial amplitude only. A procedure to handle arbitrary six-dimensional strain loops using a spectral analysis has been proposed by Niemunis et al. [5]. The stress-dependence (the increase of $\dot{\varepsilon}^{\mathrm{acc}}$ with decreasing average mean pressure p^{av} and with increasing average stress ratio $\eta^{\mathrm{av}} = q^{\mathrm{av}}/p^{\mathrm{av}}$) is captured by the functions f_p and f_Y while f_e increases $\dot{\varepsilon}^{\mathrm{acc}}$ with increasing void ratio e. The function $\dot{f}_N = \dot{f}_N^A + \dot{f}_N^B$ (see Table 1) describes the dependence of $\dot{\varepsilon}^{\mathrm{acc}}$ on cyclic preloading (historiotropy, fabric effects). The model counts the cycles weighting their number with the amplitude. Such cyclic preloading is quantified by

$$g^A = \int f_{\mathrm{ampl}}\ \dot{f}_N{}^A\ \mathrm{d}N \tag{8}$$

and used in $\dot{f}_N$. For a constant amplitude the HCA model predicts accumulation curves $\varepsilon^{\mathrm{acc}}(N)$ proportional to $f_N = C_{N1}[\ln(1+C_{N2}N)+C_{N3}N]$. Physically g^A can be seen as a measure of the arrangement of grains rendering sand more resistant against cyclic loading. The function f_π increases the accumulation rate due to changes of the polarization, see [4]. This function is not further used here since only tests with a constant polarization have been performed (i.e. $f_\pi = 1$ holds). The constants of the HCA model for a medium coarse sand determined from drained tests with $N_{\max} = 10^5$ cycles are summarized in the third column of Table 1.

Function	HCA model constants for $N_{\max}$ =		
		10^5	200
$f_{\mathrm{ampl}} = \min\left\{\left(\frac{\varepsilon^{\mathrm{ampl}}}{\varepsilon_{\mathrm{ref}}^{\mathrm{ampl}}}\right)^{C_{\mathrm{ampl}}};\ 100\right\}$	$\varepsilon_{\mathrm{ref}}^{\mathrm{ampl}}$	10^{-4}	
	C_{ampl}	2.0	1.5
$\dot{f}_N = \dot{f}_N^A + \dot{f}_N^B$	C_{N1}	$3.6 \cdot 10^{-4}$	$1.97 \cdot 10^{-4}$
$\dot{f}_N^A = C_{N1}C_{N2}\exp\left[-\frac{g^A}{C_{N1}f_{\mathrm{ampl}}}\right]$	C_{N2}	0.43	0.24
$\dot{f}_N^B = C_{N1}C_{N3}$	C_{N3}	$5.0 \cdot 10^{-5}$	$3.5 \cdot 10^{-3}$
$f_p = \exp\left[-C_p\ \left(\frac{p^{\mathrm{av}}}{p_{\mathrm{ref}}} - 1\right)\right]$	C_p	0.43	0.025
	p_{ref}	100 kPa	
$f_Y = \exp\left(C_Y\ \bar{Y}^{\mathrm{av}}\right)$	C_Y	2.0	
$f_e = \frac{(C_e - e)^2}{1+e}\ \frac{1+e_{\mathrm{ref}}}{(C_e - e_{\mathrm{ref}})^2}$	C_e	0.54	
	e_{ref}	0.874	

Table 1: Summary of the functions, reference quantities and constants of the HCA model for a medium coarse sand; the constants for $N_{\max} = 10^5$ were taken from [11], the constants for $N_{\max} = 200$ were derived in this study, Section 6

The multiplicative approach for $\dot{\varepsilon}^{\mathrm{acc}}$ in Eq. (7) was chosen heuristically and then to some extent confirmed experimentally [10,11,13]. For example, f_{ampl} was found valid for two different average stresses, one with triaxial compression ($p^{\mathrm{av}} = 200$ kPa, $\eta^{\mathrm{av}} = 0.75$) and the other one with triaxial extension ($p^{\mathrm{av}} = 200$ kPa, $\eta^{\mathrm{av}} = $ -0.5). The function f_Y was confirmed for different average mean pressures 50 kPa $\le p^{\mathrm{av}} \le$ 300 kPa and the function f_p was found valid for different average stress ratios $-0.5 \le \eta^{\mathrm{av}} \le 1.313$, although the constants C_p and C_Y may slightly vary.

For axisymmetric element tests it is convenient to rewrite Eq. (1) with Roscoe's invariants:

$$\begin{bmatrix} \dot{p} \\ \dot{q} \end{bmatrix} = \begin{bmatrix} K & 0 \\ 0 & 3G \end{bmatrix} \begin{bmatrix} \dot{\varepsilon}_v - \dot{\varepsilon}^{\mathrm{acc}}\ m_v \\ \dot{\varepsilon}_q - \dot{\varepsilon}^{\mathrm{acc}}\ m_q \end{bmatrix} \tag{9}$$

Omitting $\dot{\boldsymbol{\varepsilon}}^{\mathrm{pl}}$ in Eq. (1) is legitimate for homogeneous stress fields. The bulk modulus $K = \frac{E}{3(1-2\nu)}$ and shear modulus $G = \frac{E}{2(1+\nu)}$ are expected to be pressure-dependent. The volumetric (m_v) and the deviatoric (m_q) portions of the flow rule are:

$$\begin{bmatrix} m_v \\ m_q \end{bmatrix} = \frac{1}{\sqrt{\frac{1}{3}\left(p - \frac{q^2}{M^2 p}\right)^2 + 6\left(\frac{q}{M^2}\right)^2}} \begin{bmatrix} p - \frac{q^2}{M^2 p} \\ 2\frac{q}{M^2} \end{bmatrix} \tag{10}$$

In a drained test with stress-controlled cycles, Eq. (10) corresponds to the ratio of the rates of volumetric and deviatoric strain predicted by the well-known formula of the

MCC model:

$$\frac{\dot{\varepsilon}_v^{\mathrm{acc}}}{\dot{\varepsilon}_q^{\mathrm{acc}}} = \frac{m_v}{m_q} = \frac{M^2-(\eta^{\mathrm{av}})^2}{2\eta^{\mathrm{av}}}. \quad (11)$$

4 Determination of elastic constants

The bulk modulus K can be experimentally obtained from a comparison of the rate $\dot{u}$ of pore pressure accumulation in an undrained cyclic triaxial test and the rate $\dot{\varepsilon}_v$ of volumetric strain accumulation in a drained cyclic test with similar initial stress and initial void ratio and with the same cyclic loading. For an isotropic stress ($q = 0$, $\dot{q} = 0$, $m_q = 0$) Eq. (9) takes either the form of isotropic relaxation (see the average effective stress path in Fig. 2a)

$$\dot{p} = -K\,\dot{\varepsilon}^{\mathrm{acc}}\,m_v \quad (12)$$

under undrained conditions ($\dot{\varepsilon}_v = 0$) or the form of volumetric creep

$$\dot{\varepsilon}_v = \dot{\varepsilon}^{\mathrm{acc}}\,m_v \quad (13)$$

under drained conditions ($\dot{p} = 0$). Comparing these equations one may eliminate $\dot{\varepsilon}^{\mathrm{acc}}\,m_v$ and obtain

$$K = -\frac{\dot{p}}{\dot{\varepsilon}_v} \quad \text{or} \quad \frac{\dot{u}}{\dot{\varepsilon}_v} \quad (14)$$

For a determination of Poisson's ratio ν the effective stress evolution ($\dot{p}$,$\dot{q}$) observed in a strain-controlled undrained cyclic triaxial test commenced at an anisotropic initial stress may be compared with the prediction of Eq. (9). For $\dot{\varepsilon}_v = 0$ and $\dot{\varepsilon}_1 = 0$ and therefore $\dot{\varepsilon}_q = 0$ one obtains:

$$\begin{bmatrix} \dot{p} \\ \dot{q} \end{bmatrix} = \begin{bmatrix} K & 0 \\ 0 & 3G \end{bmatrix} \begin{bmatrix} -\dot{\varepsilon}^{\mathrm{acc}}\,m_v \\ -\dot{\varepsilon}^{\mathrm{acc}}\,m_q \end{bmatrix} \quad (15)$$

The ratio of the relaxation rates

$$\frac{\dot{q}}{\dot{p}} = \frac{3G}{K}\,\frac{m_q}{m_v} = \frac{9(1-2\nu)}{2(1+\nu)}\,\frac{2\eta^{\mathrm{av}}}{M^2-(\eta^{\mathrm{av}})^2} \quad (16)$$

depends on ν. Stress paths for different ν-values are plotted exemplary in Fig. 2b. The stress relaxates until $\boldsymbol{\sigma}' = \mathbf{0}$ is reached. Note that the deviatoric relaxation $\dot{q}$ rapidly increases with stress ratio $\eta = q/p$. The Poisson's ratio ν can be determined from the measured $\dot{q}/\dot{p}$ or judged by a curve-fitting of the experimental data using Fig. 2b.

5 Tested material, test device, specimen preparation procedure and testing program

The drained and the undrained cyclic tests were performed on a medium coarse quartz sand with subangular grain shape. The mean grain size and the coefficient of uniformity are $d_{50} = 0.55$ mm and $C_u = d_{60}/d_{10} = 1.8$, respectively. The grain size distribution curve is given for example in [10] (denoted as "Sand No. 3"). The minimum and maximum void ratios $e_{\min} = 0.577$ and $e_{\max} = 0.874$ have been determined according to German standard code DIN 18126.

A scheme of the test device is shown in Fig. 3. The axial load was applied with a pneumatic loading system. It was measured with a load cell located below the specimen base pedestal. Axial deformations of the specimen were measured with a displacement transducer mounted to the load piston. Volume changes were determined via the pore water using a pipette system in combination with a differential pressure transducer. Two pressure transducers were used to monitor pore and cell pressure. All signals were continuously recorded with a data acquisition system.

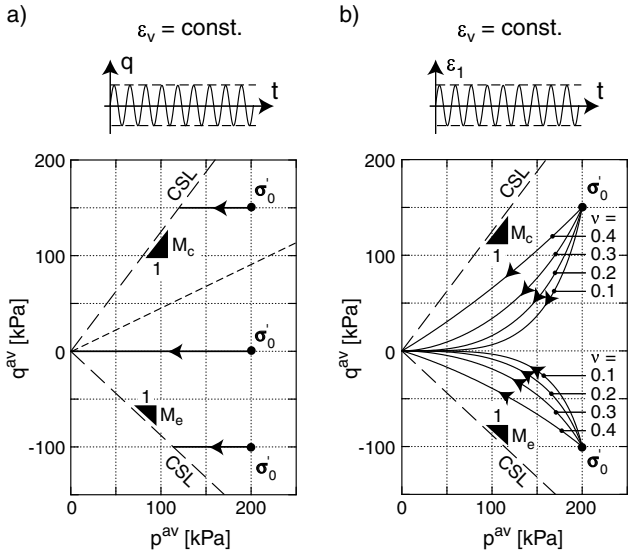

Fig. 2: *Schematic illustration of the trend of effective stress $\boldsymbol{\sigma}'$ in undrained cyclic triaxial tests with a) stress control and b) strain control*

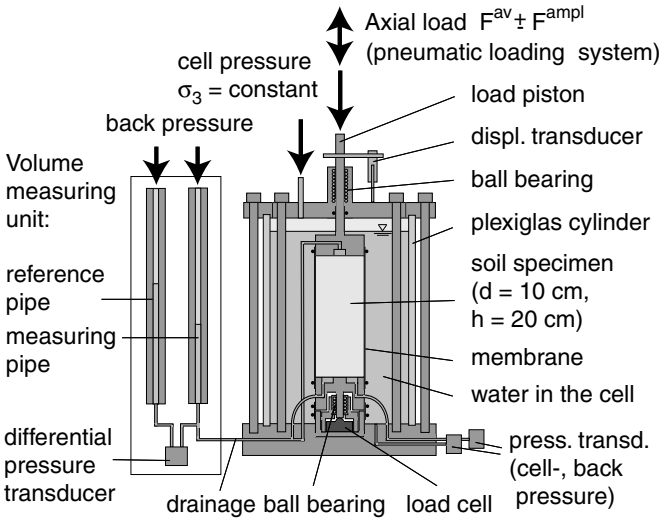

Fig. 3: *Scheme of the cyclic triaxial device used for the present study*

Specimens were prepared by pluviating dry sand out of a funnel through air into split moulds. An initial relative density of $I_{D0} = (e_{\max} - e)/(e_{\max} - e_{\min}) \approx 0.6$ was intended in all tests. After having mounted the pressure cell the specimens were flushed with carbon dioxide and afterwards saturated with de-aired water. A back pressure of 200 kPa was applied in all tests. The quality of saturation was checked by determining Skempton's B-value. $B > 0.97$ was achieved for all specimens. Subsequently the effective stress was increased isotropically to the intended initial value of the test. After a short resting period of 30

minutes the cyclic axial loading was applied using a triangular load pattern. The cell pressure was kept constant during the cycles.

In all tests (drained *and* undrained) the first cycle was applied under the drained condition. The first cycle may be irregular and may generate much more deformation than the subsequent ones. The HCA model predicts only the accumulation due to the subsequent regular cycles (see Figure 1). In numerical calculations with the HCA model the first cycle is calculated using a conventional implicit constititutive model (we use for example hypoplasticity with intergranular strain [3,9]). Since the initial conditions at the beginning of the regular cycles (initial stress and initial relative density) were intended to be similar in the drained and in the undrained tests, the first cycle was applied drained in both types of tests. In the undrained tests the drainage was closed after the first cycle and all subsequent cycles were applied undrained. The time period of a cycle was $T = 100$ s. The first cycle is not included in the following evaluation of the "elastic" stiffness E. In all diagrams $N = 1$ refers to the first regular cycle.

In the undrained tests five different initial effective pressures $p_0 = 50$, 100, 150, 200 or 300 kPa were used. The same values were used for the average mean pressure p^{av} in the drained tests. For each pressure three tests with different amplitude-pressure ratios $\zeta = q^{\mathrm{ampl}}/p_0$ (or $q^{\mathrm{ampl}}/p^{\mathrm{av}}$) $= 0.2$, 0.3 and 0.4 were conducted, that means a total number of 15 undrained and 15 corresponding drained cyclic tests were performed. The testing program is summarized in Table 2.

Most of the undrained cyclic tests were stopped when a certain amount of excess pore water pressure was reached keeping the effective stress far away from the failure line (known from undrained monotonic tests [15]). In some tests, however, the undrained cyclic loading was continued until the stress path reached the failure line or even $\boldsymbol{\sigma}' = \mathbf{0}$, that means after the stress path had reached the first loop of "cyclic mobility". Undrained tests with several such cyclic mobility loops on the same sand have been reported by Wichtmann et al. [15]. The maximum number of cycles in the drained tests was chosen similar to that applied in the corresponding undrained test.

6 Results of drained and undrained cyclic tests

In the undrained stress-controlled tests the accumulation of pore water pressure u was accompanied by the decrease of the effective axial and lateral stresses σ_1' and σ_3' (see a typical test result in Fig. 4). For $q^{\mathrm{ampl}} =$ constant the amplitude of axial strain $\varepsilon_1^{\mathrm{ampl}}$ gradually increased with N due to the decrease of p and the pressure-dependence of the secant stiffness (Fig. 5). The rapid increase of $\varepsilon_1^{\mathrm{ampl}}$ at $t \approx 2{,}700$ s corresponds to the "initial liquefaction" (i.e. $u/\sigma_3 = 1$ was reached for the first time). In accordance with the flow rule in Eq. (4) the accumulation is almost perfectly isotropic that means $\dot{\varepsilon}_q^{\mathrm{acc}} \approx 0$ for $q = 0$.

The effective stress paths of all 15 undrained cyclic tests are given in Fig. 6. Fig. 7 presents the corresponding pore water pressures $u(t)$ and the trends of pore water pressure $u(N)$ (i.e. the residual values after each cycle at $q = 0$) for different p_0- and $\zeta = q^{\mathrm{ampl}}/p_0$-values. For a certain value of p_0, the rate of pore water pressure accumulation $\dot{u}$ considerably increases with increasing stress amplitude q^{ampl}.

Test pair No.	p_0 [kPa]	q^{ampl} [kPa]	ζ [-]	Undrained I_{D0} [-]	Undrained e_0 [-]	Drained I_{D0} [-]	Drained e_0 [-]
1	50	10	0.2	0.59	0.701	0.59	0.700
2	50	15	0.3	0.59	0.700	0.61	0.692
3	50	20	0.4	0.57	0.705	0.58	0.703
4	100	20	0.2	0.61	0.693	0.61	0.694
5	100	30	0.3	0.59	0.699	0.59	0.700
6	100	40	0.4	0.60	0.696	0.60	0.695
7	150	30	0.2	0.59	0.698	0.61	0.694
8	150	45	0.3	0.61	0.693	0.61	0.693
9	150	60	0.4	0.60	0.696	0.60	0.697
10	200	40	0.2	0.62	0.690	0.60	0.697
11	200	60	0.3	0.59	0.699	0.63	0.688
12	200	80	0.4	0.64	0.685	0.61	0.694
13	300	60	0.2	0.61	0.693	0.63	0.686
14	300	90	0.3	0.63	0.687	0.62	0.690
15	300	120	0.4	0.62	0.692	0.62	0.690

Table 2: Testing program: consolidation pressure p_0, stress amplitude q^{ampl}, amplitude-pressure ratio $\zeta = q^{\mathrm{ampl}}/p_0$, initial relative density I_{D0} and initial void ratio e_0 (all tests: $q_0 = 0$)

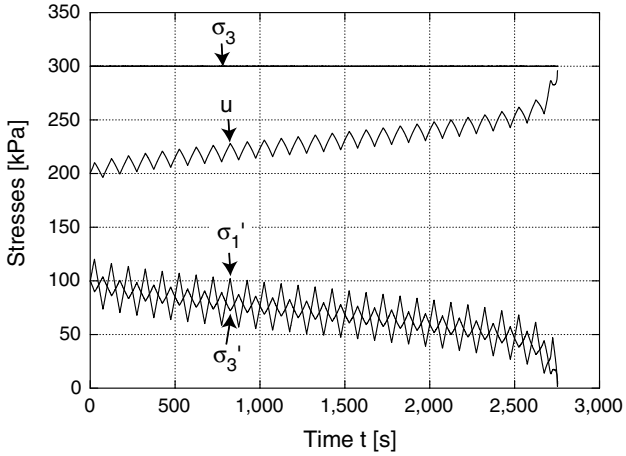

Fig. 4: *Stresses $\sigma_3(t)$, $u(t)$, $\sigma_1'(t)$ and $\sigma_3'(t)$ versus time in an undrained test with $p_0 = 100$ kPa, $q_0 = 0$ and $\zeta = 0.3$ (Test No. 5 in Table 2)*

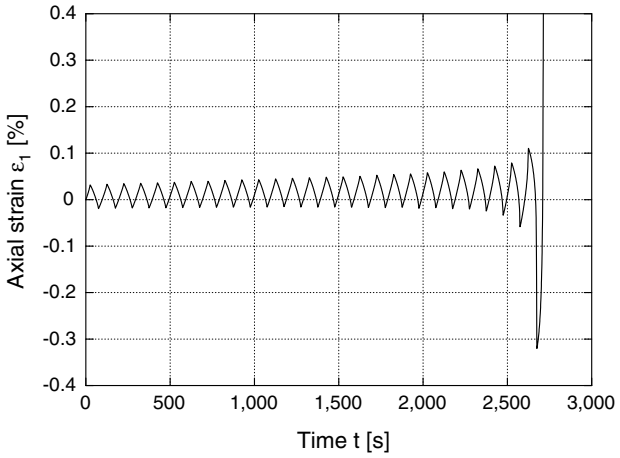

Fig. 5: *Axial strain $\varepsilon_1(t)$ versus time in an undrained test with p_0 = 100 kPa, q_0 = 0 and ζ = 0.3 (Test No. 5 in Table 2)*

The relaxation of the effective mean stress p is accompanied by an increase of the strain amplitude $\varepsilon^{\mathrm{ampl}} = \sqrt{3/2}\,\varepsilon_1^{\mathrm{ampl}}$ (Fig. 7).

The measured accumulation of strain during stress cycles in drained tests is almost perfectly isotropic ($\dot{\varepsilon}_q^{\mathrm{acc}} \approx 0$, $\dot{\varepsilon}_v^{\mathrm{acc}} \neq 0$, see a typical result in Fig. 8), which is in accordance with the flow rule Eq. (4). Analogous results for different p^{av}- and ζ-values are given in Fig. 9 as a strain path $\varepsilon_v(t)$ and as a trend $\varepsilon_v^{\mathrm{acc}}(N)$. For a constant p^{av}, the creep rate $\dot{\varepsilon}_v^{\mathrm{acc}}$ increases with the stress amplitude q^{ampl}. The strain amplitude $\varepsilon^{\mathrm{ampl}}$ moderately decreased during the first cycles, especially for the larger amplitude-pressure ratios (Fig. 9).

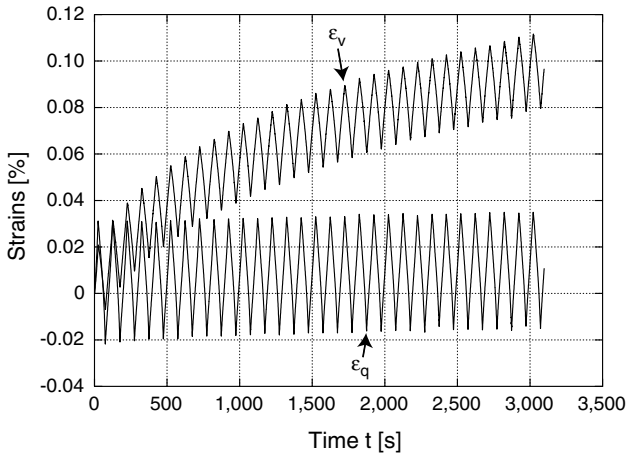

Fig. 8: *Volumetric strain $\varepsilon_v(t)$ and deviatoric strain $\varepsilon_q(t)$ versus time in a drained test with p^{av} = 100 kPa, q^{av} = 0 and ζ = 0.3 (Test No. 5 in Table 2)*

7 Evaluation of bulk modulus $K = \dot{u}/\dot{\varepsilon}_v^{\mathbf{acc}}$

For each pair of drained and undrained cyclic tests the bulk modulus K was calculated from Eq. (14). The rates $\dot{u}$ and $\dot{\varepsilon}_v^{\mathrm{acc}}$ were calculated from the trend curves $u(N)$ and $\varepsilon_v^{\mathrm{acc}}(N)$ given in Figs. 7 and 9.

During an undrained cyclic test with q^{ampl} = constant the average mean pressure decreases and the strain amplitude $\varepsilon^{\mathrm{ampl}}$ increases considerably due to the pressure-dependence of the secant stiffness. In the drained test p^{av} is constant and the strain amplitude does not change much, but the void ratio e decreases with N which affects the rate of accumulation via f_e (Table 1). In order to evaluate $\dot{u}$ and $\dot{\varepsilon}_v^{\mathrm{acc}}$ for exactly the same test conditions that means same values of $\varepsilon^{\mathrm{ampl}}$, e, p^{av} and N (strictly speaking g^A, Eq. (8)), the rate $\dot{\varepsilon}_v^{\mathrm{acc}}$ from the drained tests was corrected by a factor f_c consisting of four multipliers:

$$f_c = \frac{f_{\mathrm{ampl}}^{UD}}{f_{\mathrm{ampl}}^{D}} \frac{f_e^{UD}}{f_e^{D}} \frac{f_p^{UD}}{f_p^{D}} \frac{\dot{f}_N^{UD}}{\dot{f}_N^{D}} \tag{17}$$

with the functions f_{ampl}, f_e, f_p and $\dot{f}_N$ given in Table 1. The indices $\sqcup^{UD}$ and $\sqcup^{D}$ indicate the undrained or drained test, respectively.

In [11] it has been demonstrated that the dependence of the intensity of accumulation $\dot{\varepsilon}^{\mathrm{acc}}$ on the average mean pressure p^{av} becomes more pronounced with increasing number of cycles (i.e. the parameter C_p in f_p increases with N). In many test pairs performed for the present study the number of cycles did not exceed $N = 50$ (due to the fast accumulation of pore water pressure in the undrained test). In none of the tests the maximum number of cycles was larger than 1,000. In order to improve the accuracy of f_c, based on the data from the 15 drained tests the parameters of the functions f_{ampl}, f_p and $\dot{f}_N$ were determined. The void ratio function f_e could not be inspected since the initial void ratio did not differ significantly in the present test series. Thus, $C_e = 0.54$ obtained from another test series with $N = 10^5$ cycles [11] had to be applied in the present analysis.

The residual volumetric strain $\varepsilon_v^{\mathrm{acc}}$ after N = 10 or 20 cycles, respectively, increases over-proportionally with the strain amplitude, Figure 10a. On the abscissa a mean value of the strain amplitude $\bar{\varepsilon}^{\mathrm{ampl}} = 1/N \int \varepsilon^{\mathrm{ampl}}(N)\,\mathrm{d}N$ is used. In order to consider the slightly different initial void ratios e_0 and different compaction rates $\dot{e} = \partial e/\partial N$, on the ordinate the residual volumetric strain has been divided by the void ratio function $\bar{f}_e$. It has been calculated with a mean value of the void ratio $\bar{e} = 1/N \int e(N)\,\mathrm{d}N$. The exponent $C_{\mathrm{ampl}} = 1.5$ of the relationship $\dot{\varepsilon}^{\mathrm{acc}} \sim (\varepsilon^{\mathrm{ampl}})^{C_{\mathrm{ampl}}}$ (function f_{ampl}, Table 1) is lower than $C_{\mathrm{ampl}} = 2.0$ observed in tests with $\eta^{\mathrm{av}} = 0.75$ for various sands and various N-values [14].

The pressure-dependence of the accumulation rate is quite low at low N-values, Fig. 10b. Note that the HCA model disregards the N-dependence of f_p for the sake of simplicity. In Fig. 10b, the data has been divided by $\bar{f}_{\mathrm{ampl}}$ and $\bar{f}_e$ in order to remove the influences of strain amplitude and void ratio. A mean value $C_p = 0.025$ has been used in the function f_p for calculating the correction factor in Eq. (17).

The "distilled" accumulation curves $\varepsilon_v^{\mathrm{acc}}(N)/(\bar{f}_{\mathrm{ampl}}\bar{f}_e f_p f_Y)$ with $f_Y = 1$ from the 15 drained tests can be approximated by the function $\sqrt{3}\ f_N = \sqrt{3}\ C_{N1}[\ln(1 + C_{N2}N) + C_{N3}N]$ with $C_{N1} = 1.97 \cdot 10^{-4}$, $C_{N2} = 0.24$ and $C_{N3} = 3.51 \cdot 10^{-3}$, Figure 10c. All constants of the HCA model derived from the data of the present study are summarized in the fourth column of Table 1.

The data from the undrained tests has to be corrected because of membrane penetration effects (system compli-

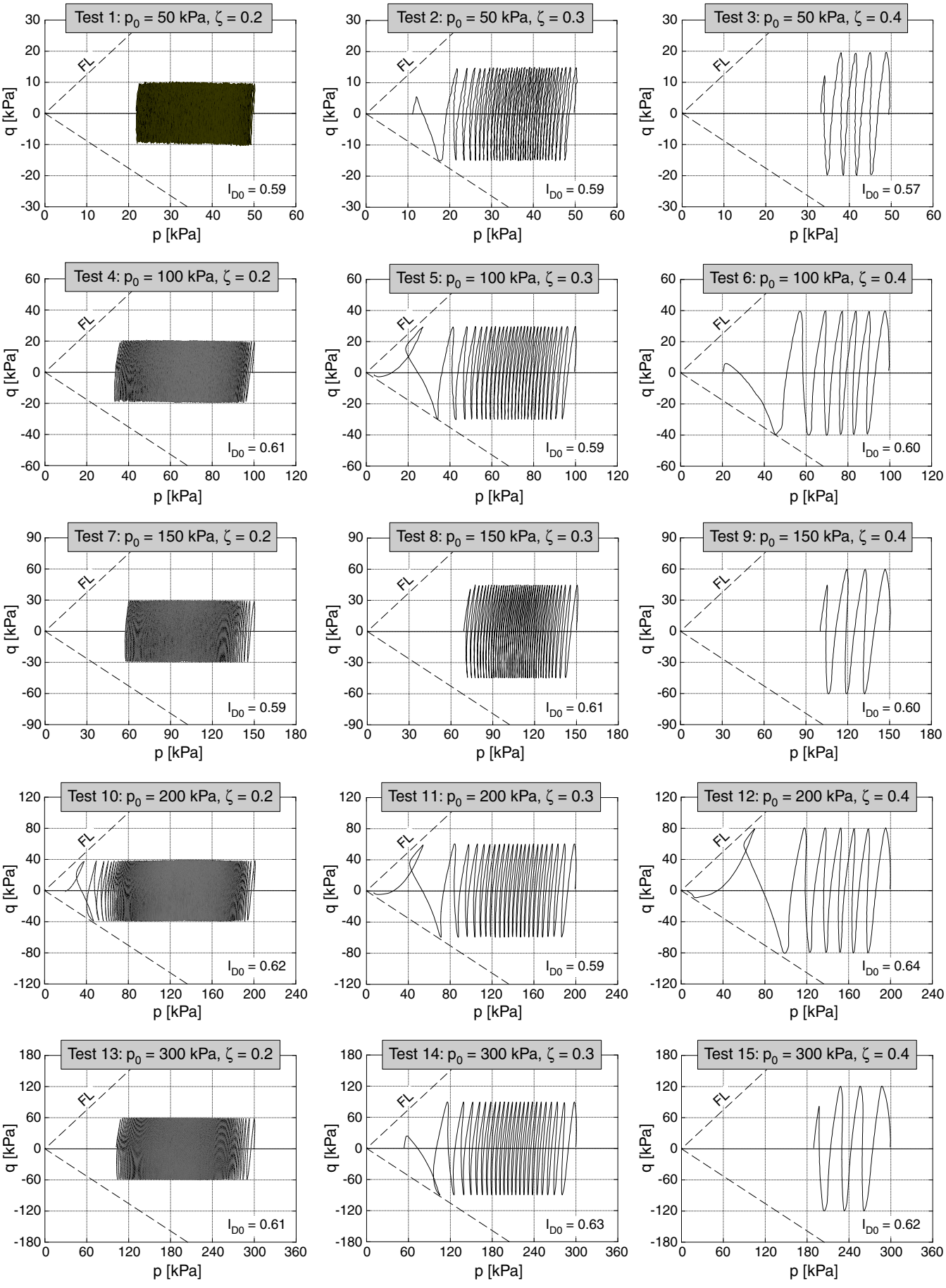

Fig. 6: *Effective stress paths in the p-q-plane measured in the 15 undrained cyclic tests*

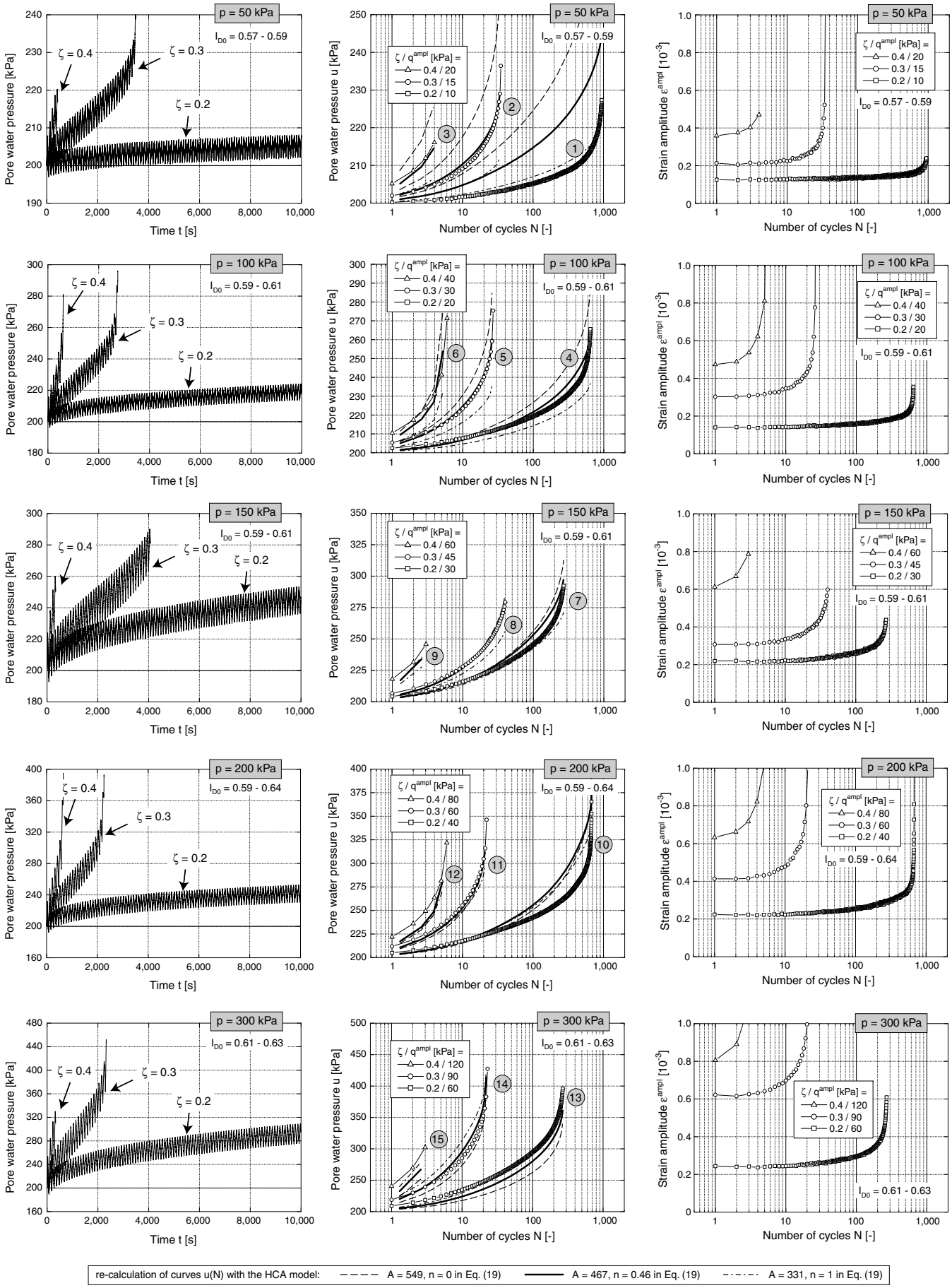

Fig. 7: *Results of the 15 undrained cyclic tests: Left: Development of pore water pressure u with time t, Middle: Residual value of u as a function of the number of cycles N, Right: Strain amplitude ε^{ampl} as a function of the number of cycles N*

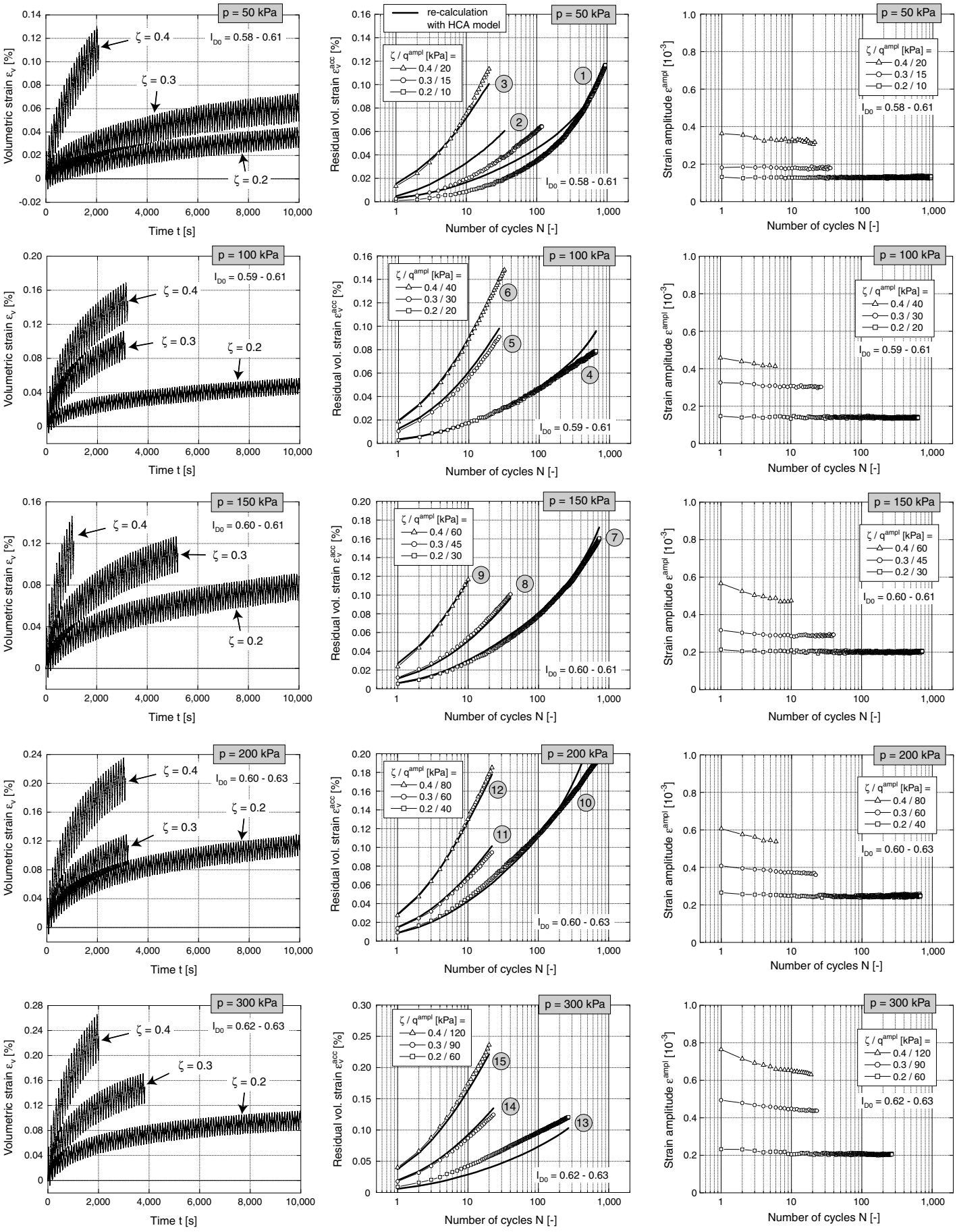

Fig. 9: *Results of the 15 drained cyclic tests: Left: Development of volumetric strain ε_v with time t, Middle: Residual strain ε_v^{acc} as a function of the number of cycles N, Right: Strain amplitude ε^{ampl} as a function of the number of cycles N*

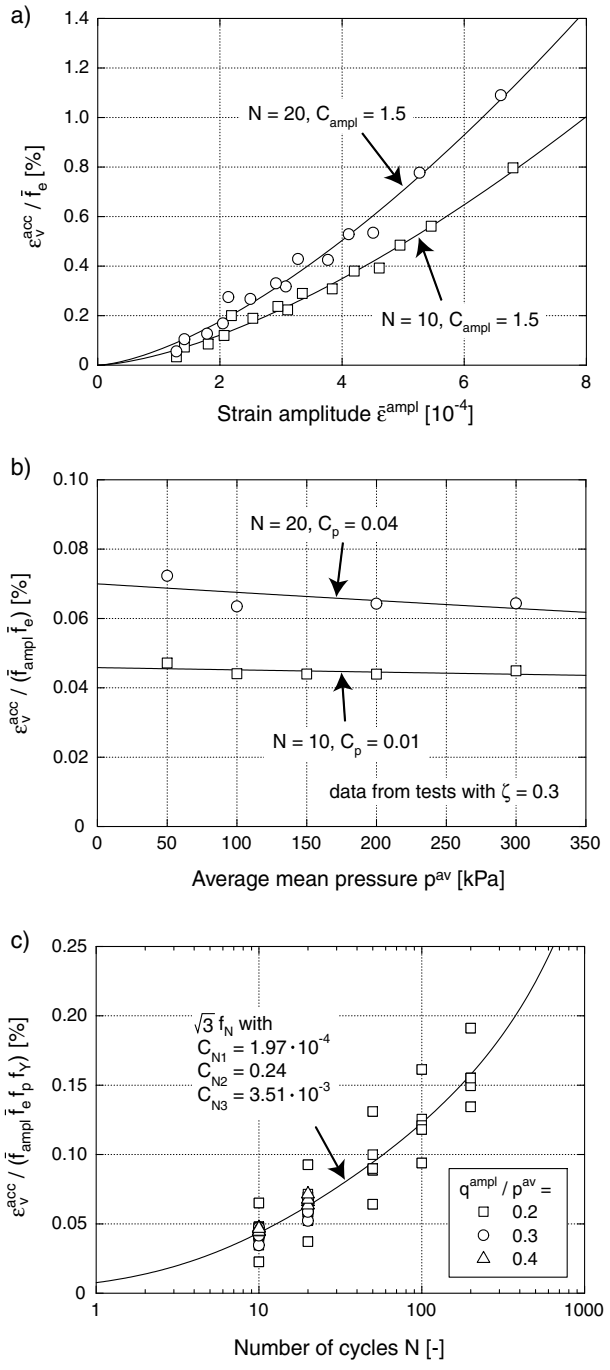

Fig. 10: *Residual volumetric strain ε_v^{acc} measured in the 15 drained cyclic tests a) normalized by the void ratio function $\bar{f}_e$ and plotted versus strain amplitude $\bar{\varepsilon}^{ampl}$, b) normalized by $\bar{f}_e$ and by the amplitude function $\bar{f}_{ampl}$ versus average mean pressure p^{av}, c) normalized by $\bar{f}_e$, $\bar{f}_{ampl}$ and by the stress functions f_p and f_Y versus number of cycles N*

ance). The increase of pore water pressure due to cyclic loading and the accompanying decrease of the effective lateral stress σ_3' lead to a reduction of the penetration of the rubber membrane into the voids at the boundary of the specimen. This implies a slight increase of the volume of the specimen (i.e. $\Delta V \neq 0$) and thus a slower accumulation of the pore water pressure (for a detailed discussion consult Nicholson et al. [1] or Sivathayalan & Vaid [7]). In the present study a correction method proposed by Tokimatsu [8] has been used, Fig. 11. In order to obtain the true material response, that means data free from membrane penetration effects, the N-axis is scaled by a factor $1/C_N$ with

$$C_N = \exp(1.77\, C_R) \quad \text{and} \quad C_R = \frac{B}{3\,\frac{u^{\text{ampl}}}{q^{\text{ampl}}}} \tag{18}$$

(derived from Fig. 10 in [8]) with C_R and B being the system compliance ratio and Skempton's B-value, respectively. The ratio $u^{\text{ampl}}/q^{\text{ampl}}$ of the amplitudes of pore water pressure and deviatoric stress amplitude is obtained from the middle stage of an undrained test. An analysis of the data of the 15 undrained tests performed in the present study delivered a mean value $C_N = 1.30$. Before evaluating K according to Eq. (14) the curves $u(N)$ of all undrained tests have been scaled by $1/C_N$.

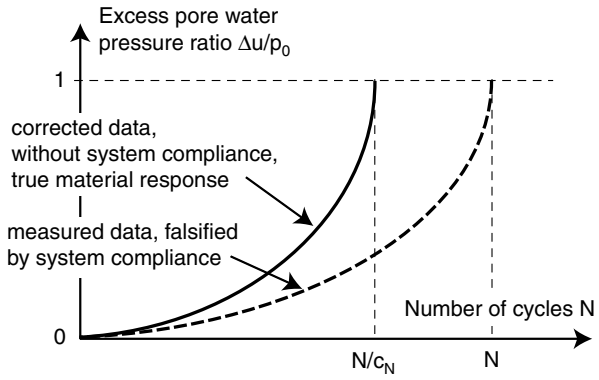

Fig. 11: *Correction of the measured trend $u(N)$ of pore water pressure with respect to membrane penetration effects (system compliance), method proposed by Tokimatsu [8]*

The bulk modulus K was determined over the range of $\Delta u = 10$ kPa. Data for which one of the four multipliers in Eq. (17) was larger than 2.0 or for which the strain amplitude exceeded $\varepsilon^{\text{ampl}} = 10^{-3}$ were omitted. Only small strain amplitudes $\varepsilon^{\text{ampl}} \leq 10^{-3}$ were accepted for the evaluation of K due to limitations in the HCA model [4, 10].

Fig. 12 presents the bulk modulus K versus average mean pressure p^{av}. The data from all 15 pairs of tests fall into a concentrated cloud of points, although especially the data for the small amplitudes ($\zeta = 0.2$) show some scatter. The obvious pressure-dependence of K can be approximated by

$$K = A\, p_{\text{atm}}^{1-n}\, p^n \tag{19}$$

with $A = 467$ and $n = 0.46$ (the fat solid line in Fig. 12). In the recalculations of the undrained cyclic tests presented in the next section also a constant bulk modulus $K = 54.9$ MPa (corresponding to $A = 549$ and $n = 0$ in Eq. (19), see the fat dashed line in Fig. 12) and a linear relationship (A

= 331 and $n = 1$, see the fat dot-dashed line in Fig. 12) were tried out. The constant bulk modulus is the mean value of all data in Fig. 12.

The data for the large amplitude-pressure ratio $\zeta = 0.4$ lay at the upper boundary of the cloud of data in Fig. 12 while the data for $\zeta = 0.2$ are located at the lower boundary. However, this slight amplitude-dependence may be neglected for practical purpose.

The data in Figure 12 gives no evidence that K depends on cyclic preloading (i.e. on the number of cycles N). Hence, a conclusion of an earlier publication has to be revised. In [16] the data from drained and undrained cyclic tests has been analyzed using the constants in the third column of Table 1 (i.e. the constants determined from tests with a large number of cycles) and no correction for membrane penetration effects was applied.

8 Numerical simulation of element tests with the HCA model

The good approximation of the experimental data from the drained tests by the HCA model with the constants in the fourth column of Table 1 is demonstrated in the middle column of diagrams in Fig. 9 where the predicted trend curves $\varepsilon_v^{\mathrm{acc}}(N)$ have been added (solid lines). The initial void ratios and the measured curves of the strain amplitude $\varepsilon^{\mathrm{ampl}}(N)$ were used as an input for the recalculations. Despite some deviations for $p^{\mathrm{av}} = 50$ kPa and for amplitude-pressure ratios of $\zeta = 0.2$ and 0.3, the measured and the predicted curves agree well.

The undrained cyclic tests have been recalculated using the HCA model with K obtained from Eq. (19) and with the constants given in the fourth column of Table 1. The initial void ratios and the measured curves of the strain amplitude $\varepsilon^{\mathrm{ampl}}(N)$ were used as an input. In contrast to the experimental data the curves $u(N)$ predicted by the HCA model are free from membrane penetration effects. Therefore, for comparison purpose the N-axis has been scaled by a factor 1.3 (therefore the predicted curves start at $N = 1.3$).

Three different pairs of constants A and n in Eq. (19) were tried out. The constants $A = 467$ and $n = 0.46$ approximate well the pressure-dependence of the data in Fig. 12. Using these constants, the trend $u(N)$ predicted by the HCA model agrees quite well with the experimental data (see the middle column of diagrams in Fig. 7), except a large deviation in case of the test with $p_0 = 50$ kPa and $\zeta = 0.2$. The surprisingly low accumulation of pore water pressure in the test with $p^{\mathrm{av}} = 50$ kPa and $\zeta = 0.2$ may be due to preloading or aging effects since an effective stress of 50 kPa was also applied during the specimen preparation procedure. While these effects may not influence the accumulation at larger amplitudes and pressures, they may have reduced the rates $\dot{u}$ for the small amplitude-pressure ratio $\zeta = 0.2$.

For FE calculations a constant bulk modulus ($A = 549$ and $n = 0$) or a linear relationship ($A = 331$ and $n = 1$) would be advantageous for numerical reasons. The constant value overestimates the bulk modulus at small pressures and underestimates it at large pressures (Fig. 12). For a linear approximation of $K(p)$ it is the other way around. Consequently, the dashed curves $u(N)$ in Fig. 7 reveal that a constant bulk modulus overestimates the accumulation of pore water pressure in the tests with small initial pressures ($p_0 = 50$ and 100 kPa) while the rate $\dot{u}$ is underestimated in the tests with a large initial pressure ($p_0 = 300$ kPa). The usage of a linear relationship for $K(p)$ results in an underestimation of the pore water pressure accumulation in the tests with initial pressures $p_0 = 50$ and 100 kPa while the prediction is still acceptable for $p_0 = 300$ kPa (dot-dashed curves in Fig. 7). For intermediate initial pressures ($p_0 = 150$ and 200 kPa) all three sets of constants for A and n deliver similar bulk moduli and thus approximate well the measured data. However, based on the predicted curves $u(N)$ in Fig. 7 it can be stated that for FE calculations involving poor drainage conditions the usage of a constant or a linear function for $K(p)$ seems to be over-simplified.

It can be concluded that the HCA model with a single set of constants (fourth column of Table 1) in combination with the pressure-dependent bulk modulus derived in the present study (Eq. (19) with $A = 467$ and $n = 0.46$) describes well both, the accumulation of pore water pressure in undrained cyclic tests and the accumulation of volumetric strain in drained cyclic tests.

9 Simplified determination of K

Judging by the presented test results a proper determination of $K(p)$ requires at least two pairs of drained and undrained cyclic tests with different initial effective mean pressures (e.g. $p_0 = 100$ and 300 kPa). The tests could be performed for example with an intermediate amplitude-pressure ratio of $\zeta = 0.3$. For coarse-grained sands membrane penetration effects may become considerable (according to Nicholson et al. [1] they increase over-proportionally with the grain size d_{20}) and the procedure discussed above may not be sufficiently accurate. Alternatively to this calibration a simplified procedure has been studied. The modulus K is estimated from oedometric or resonant column test data.

Two tests with oedometric compression (specimen diameter $d = 10$ cm, height $h = 3.5$ cm) were performed on dry sand. The initial relative density I_{D0} was 0.63 in both tests. The maximum axial stress was $\sigma_1 = 2$ MPa. A single un- and reloading cycle was performed. The evolution of void ratio e in the tests is given in Figure 13. The bulk modulus was estimated from the constrained elastic modulus $M = \Delta\sigma_1/\Delta\varepsilon_1$ using the relationship $K = \frac{1+\nu}{3(1-\nu)}M$. Curves $K(p)$ for two different values of Poisson's ratio ($\nu = 0.2$ and $\nu = 0.25$, respectively) have been added to Figure 12 (narrow dashed curves). They represent mean values of the two performed tests. In order to calculate p, the lateral stress in the oedometric tests was estimated from $\sigma_3 = K_0\sigma_1$ using Jaky's formula $K_0 = 1 - \sin\varphi_c$ with the critical friction angle $\varphi_c = 31.2°$ which was determined from a pluviated cone of sand. Figure 12 reveals that the bulk modulus from the comparison of the drained and undrained cyclic tests agrees quite well with the bulk modulus obtained from the oedometric compression tests during un- and reloading. This seems to be quite reasonable since an increase of the pore water pressure and the accompanying decrease of the effective mean pressure corresponds to an elastic unloading. Hence, the approach of Sawicki [6] could be confirmed. Therefore, a simplified procedure using merely the un- and reloading curve in an oedometric compression test provides a sufficiently exact estimate of

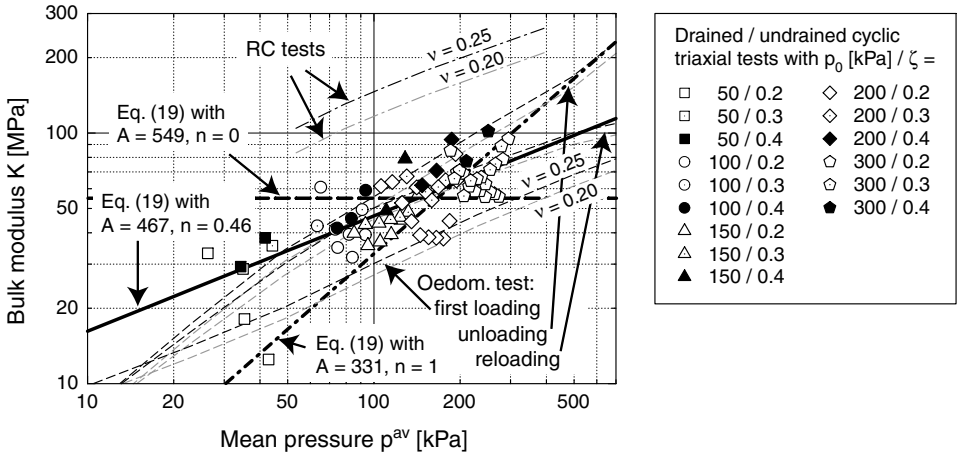

Fig. 12: *Bulk modulus $K = \dot{u}/\dot{\varepsilon}_v^{acc}$ determined from the comparison of the drained and undrained cyclic tests as a function of average mean pressure p^{av}, comparison with the data from oedometric tests and from resonant column tests*

K for engineering purposes.

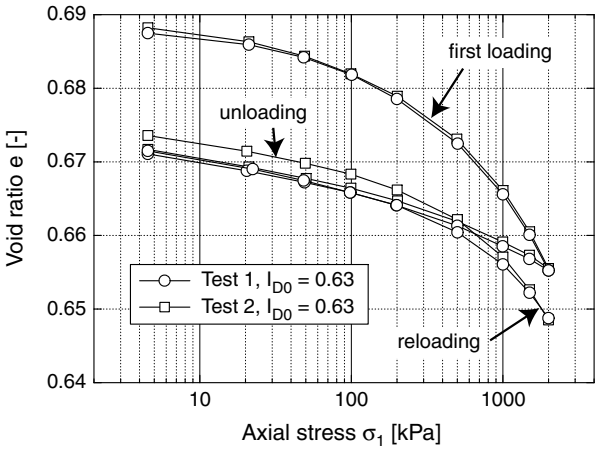

Fig. 13: *Void ratio e versus axial stress σ_1 in two tests with oedometric compression*

An estimation of K based on the small-strain shear modulus $G_{\max}$ measured at very small shear strain amplitudes $\gamma^{ampl} < 10^{-6}$ in resonant column (RC) tests turned out to be less suitable. The RC tests were performed with cylindrical specimens of dry sand (diameter 10 cm, height 20 cm). The test device is of the "free-free"-type meaning both the top and the base mass are freely rotatable [17]. $G_{\max}$ increases with pressure and decreases with void ratio (Figure 14). The small-strain bulk modulus was estimated from $K_{\max} = \frac{2(1+\nu)}{3(1-2\nu)} G_{\max}$. Curves $K_{\max}(p)$ obtained from a test with $I_{D0} = 0.57$ and for $\nu = 0.2$ and $\nu = 0.25$, respectively, have been added to Figure 12 (narrow dot-dashed curves). $K_{\max}$ from the RC test data is approximately three times larger than $K = \dot{u}/\dot{\varepsilon}_v^{acc}$ obtained from the comparison of the drained and undrained cyclic tests. The use of a small-strain stiffness for E in a HCA model would significantly overpredict stress relaxation. Resonant column tests are therefore not appropriate for a simplified determination of $K = \dot{u}/\dot{\varepsilon}_v^{acc}$.

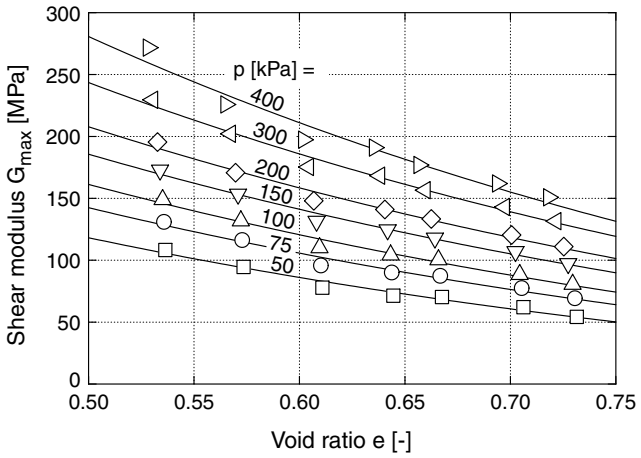

Fig. 14: *Small-strain shear modulus $G_{\max}$ as a function of void ratio e and mean pressure p, measured in resonant column tests*

10 Summary, conclusions and outlook

The paper presents an evaluation of the "elastic" stiffness E in the basic equation $\dot{\boldsymbol{\sigma}}' = \mathsf{E} : (\dot{\boldsymbol{\varepsilon}} - \dot{\boldsymbol{\varepsilon}}^{acc} - \dot{\boldsymbol{\varepsilon}}^{pl})$ of a high-cycle accumulation (HCA) model [4]. The bulk modulus K used in E was evaluated from a comparison of the rate of volumetric creep $\dot{\varepsilon}_v^{acc}$ and the rate of pore water pressure accumulation $\dot{u}$ (stress relaxation) in 15 pairs of drained and undrained cyclic triaxial tests with similar isotropic initial pressures, similar void ratios and deviatoric stress amplitudes. The experiments show that K is pressure-dependent and that it can be approximated by Eq. (19) with constants $A = 467$ and $n = 0.46$. The usage of a constant bulk modulus or a linear relationship for $K(p)$ would be over-simplified. K seems not to depend on cyclic preloading. The small amplitude-dependence can be neglected for practical purpose as it has been done in the HCA model. For a simplified procedure, K can be estimated from the un- and reloading curve in an oedometric compression test. The use of a small-strain stiffness for E would significantly overpredict stress relaxation. Recalculations of the experimental data confirmed that the HCA model [4] with a single set of constants in combination with

the bulk modulus K given by Eq. (19) describes well both, the accumulation of pore water pressure in undrained cyclic tests and the accumulation of volumetric strain in drained cyclic tests.

In future, the void-ratio dependence of K will be studied and an appropriate extension of Eq. (19) will be proposed if necessary. The minor amplitude-dependence observed in the experiments needs further inspection. Poisson's ratio ν can be evaluated from displacement-controlled undrained cyclic triaxial tests with anisotropic initial stresses (Fig. 2b). At present it is recommended to choose Poisson's ratio in the range $0.2 \leq \nu \leq 0.3$ for calculations with the HCA model.

Acknowledgements

The experimental work was done as a part of the project A8 "Influence of the fabric change in soil on the lifetime of structures", supported by the German Research Council (DFG) within the Collaborate Research Centre SFB 398 "Lifetime oriented design concepts" at Ruhr-University Bochum. The authors are indepted to DFG for this financial support.

References

[1] P.G. Nicholson, R.B. Seed, and H.A. Anwar. Elimination of membrane compliance in undrained triaxial testing. I. Measurement and evaluation. *Canadian Geotechnical Journal*, 30:727–738, 1993.

[2] A. Niemunis. Extended hypoplastic models for soils. Habilitation, Veröffentlichungen des Institutes für Grundbau und Bodenmechanik, Ruhr-Universität Bochum, Heft Nr. 34, 2003. available from www.pg.gda.pl/∼aniem/an-liter.html.

[3] A. Niemunis and I. Herle. Hypoplastic model for cohesionless soils with elastic strain range. *Mechanics of Cohesive-Frictional Materials*, 2:279–299, 1997.

[4] A. Niemunis, T. Wichtmann, and T. Triantafyllidis. A high-cycle accumulation model for sand. *Computers and Geotechnics*, 32(4):245–263, 2005.

[5] A. Niemunis, T. Wichtmann, and Th. Triantafyllidis. On the definition of the fatigue loading for sand. In *International Workshop on Constitutive Modelling - Development, Implementation, Evaluation, and Application, 12-13 January 2007, Hong Kong*, 2007.

[6] A. Sawicki. Modelling earthquake-induced phenomena in the Izmit Bay coastal area. In Th. Triantafyllidis, editor, *Cyclic Behaviour of Soils and Liquefaction Phenomena, Proc. of CBS04, Bochum, March/April 2004*, pages 431–440. Balkema, 2004.

[7] S. Sivathayalan and Y.P. Vaid. Truly undrained response of granular soils with no membrane-penetration effects. *Canadian Geotechnical Journal*, 35(5):730–739, 1998.

[8] K. Tokimatsu. System compliance correction from pore pressure response in undrained triaxial tests. *Soils and Foundations*, 30(2):14–22, 1990.

[9] P.-A. von Wolffersdorff. A hypoplastic relation for granular materials with a predefined limit state surface. *Mechanics of Cohesive-Frictional Materials*, 1:251–271, 1996.

[10] T. Wichtmann. Explicit accumulation model for non-cohesive soils under cyclic loading. PhD thesis, Publications of the Institute of Soil Mechanics and Foundation Engineering, Ruhr-University Bochum, Issue No. 38, available from www.rz.uni-karlsruhe.de/∼gn97/, 2005.

[11] T. Wichtmann, A. Niemunis, and T. Triantafyllidis. Strain accumulation in sand due to cyclic loading: drained triaxial tests. *Soil Dynamics and Earthquake Engineering*, 25(12):967–979, 2005.

[12] T. Wichtmann, A. Niemunis, and T. Triantafyllidis. On the influence of the polarization and the shape of the strain loop on strain accumulation in sand under high-cyclic loading. *Soil Dynamics and Earthquake Engineering*, 27(1):14–28, 2007.

[13] T. Wichtmann, A. Niemunis, and T. Triantafyllidis. Strain accumulation in sand due to cyclic loading: drained cyclic tests with triaxial extension. *Soil Dynamics and Earthquake Engineering*, 27(1):42–48, 2007.

[14] T. Wichtmann, A. Niemunis, and T. Triantafyllidis. Validation and calibration of a high-cycle accumulation model based on cyclic triaxial tests on eight sands. *Soils and Foundations*, 49(5):711–728, 2009.

[15] T. Wichtmann, A. Niemunis, T. Triantafyllidis, and M. Poblete. Correlation of cyclic preloading with the liquefaction resistance. *Soil Dynamics and Earthquake Engineering*, 25(12):923–932, 2005.

[16] T. Wichtmann, A. Niemunis, and Th. Triantafyllidis. Recent advances in constitutive modelling of compaction of granular materials under cyclic loading. In N. Bazeos, D.C. Karabalis, D. Polyzos, D.E. Beskos, and J.T. Katsikadelis, editors, *Proc. of 8th HSTAM International Congress on Mechanics, Patras, Greece 12 14 July*, volume 1, pages 121–136. Hellenic Society for Theoretical and Applied Mechanics, Athens, 2007.

[17] T. Wichtmann and T. Triantafyllidis. On the influence of the grain size distribution curve of quartz sand on the small strain shear modulus $G_{\max}$. *Journal of Geotechnical and Geoenvironmental Engineering, ASCE*, 135(10):1404–1418, 2009.

List of symbols

B	Skempton's B-value
C_N	Membrane penetration correction factor
C_R	System compliance ratio
δ_{ij}	Kronecker's symbol
e	Void ratio
ε_1	Axial strain
ε_3	Lateral strain
ε_v	Volumetric strain
ε_q	Deviatoric strain
$\varepsilon^{\mathrm{ampl}}$	Strain amplitude
$\varepsilon^{\mathrm{acc}}$	Residual (accumulated) strain

$\dot{\varepsilon}^{\mathrm{acc}}$	Intensity of strain accumulation
$\boldsymbol{\varepsilon}$	Strain tensor
$\dot{\boldsymbol{\varepsilon}}$	Trend of strain
$\dot{\boldsymbol{\varepsilon}}^{\mathrm{acc}}$	Rate of strain accumulation
$\dot{\boldsymbol{\varepsilon}}^{\mathrm{pl}}$	Plastic strain rate
E	Young's modulus
E	Elastic stiffness tensor
φ_c	Critical friction angle
f_{ampl}	Amplitude function (HCA model)
f_c	Correction factor
f_e	Void ratio function (HCA model)
f_N	Function for cyclic preloading (HCA model)
f_p	Pressure function (HCA model)
f_Y	Stress ratio function (HCA model)
f_π	Function for polarization changes (HCA model)
F	Correction factor for M
γ^{ampl}	Shear strain amplitude
g^A	Historiotropic variable (HCA model)
G	Shear modulus
$G_{\max}$	Small strain shear modulus
η	Stress ratio
η^{av}	Average stress ratio
I_D	Relative density
K	Bulk modulus
K_0	Earth pressure coefficient at rest
λ	Lame constant
μ	Lame constant
m_v	Volumetric component of $\mathbf{m}$
m_q	Deviatoric component of $\mathbf{m}$
M	Constrained elastic modulus
M	Critical stress ratio
M_c	Critical stress ratio for triax. compr.
M_e	Critical stress ratio for triax. ext.
$\mathbf{m}$	Direction of strain accumulation
ν	Poisson's ratio
N	Number of cycles
p	Effective mean pressure
p^{av}	Average effective mean pressure
q	Deviatoric stress
q^{ampl}	Deviatoric stress amplitude
σ_1	Total axial stress
σ_1'	Effective axial stress
σ_3	Total lateral stress
σ_3'	Effective lateral stress
$\boldsymbol{\sigma}'$	Effective stress tensor
$\dot{\boldsymbol{\sigma}}'$	Trend of effective stress
u	Pore water pressure
$\bar{Y}$	Normalized stress ratio
ζ	Amplitude-pressure ratio
$\mathbf{1}$	Second-order identity tensor
I	Fourth-order identity tensor